

## A Hybrid CFD-BEM Technique Based on the Burton-Miller Formulation Applied to Aeroacoustic Scattering

P. Croaker<sup>1</sup>, M. Karimi<sup>1</sup> and N. Kessissoglou<sup>1</sup>

<sup>1</sup>School of Mechanical and Manufacturing Engineering, UNSW Australia, Sydney, Australia

### Abstract

A hybrid computational fluid dynamics (CFD) - boundary element method (BEM) technique is proposed that allows the total sound pressure field produced by low Mach number flow past a rigid body to be predicted. An incompressible CFD solver is used to calculate the transient hydrodynamic flow field. Acoustic sources based on Lighthill's acoustic analogy are extracted from the flow field data. A CFD-BEM coupling technique is then used to compute the propagation of waves from the flow noise sources to the surface of the body. The incident pressure and pressure gradient on the body is calculated based on a near-field solution of Lighthill's analogy. This incident field is then combined with a BEM model of the body to predict the scattered sound pressure field. The BEM model solves the Burton-Miller boundary integral equations to guarantee a unique solution at all frequencies. The results from this hybrid CFD-BEM technique are presented for turbulent flow past a circular cylinder, with Reynolds number  $Re_D=46,000$  and Mach number  $M=0.21$ . The computed aerodynamic and acoustic results are in good agreement with numerical results and experimental data from literature.

### Introduction

For low Mach number flows past an acoustically compact body, flow field data obtained from either a compressible or an incompressible CFD analysis will produce accurate acoustic results when used in conjunction with Curle's analogy [4]. However, if the body is not acoustically compact, Curle's analogy does not accurately predict the scattered sound field unless the compressibility of the fluid is included in the hydrodynamic analysis [13, 6]. However, for low Mach number flow induced noise simulations, it is incredibly challenging to include the fluid compressibility in the hydrodynamic analysis [13].

Khalighi et al. [6] solved a boundary integral equation developed from Lighthill's wave equation [8] using BEM. In their work, the volume distribution of quadrupole sources in the flow field act as the acoustic sources and no assumptions about the compactness of the source region is made. The approach of Khalighi et al. [6] is an excellent method for predicting low Mach number flow induced noise in the presence of both acoustically compact or non-compact bodies. One drawback however is that the propagation of the acoustic waves produced by the hydrodynamic noise sources to the body were incorporated directly in the authors's own BEM solver, which relies on the CHIEF method [12] to deal with the irregular frequencies that are encountered in exterior BEM problems. Marburg and Amini [9] show that the Burton and Miller method [1] is a more reliable and robust method to remove the irregular frequencies compared to the CHIEF method as it provides a unique solution for exterior acoustic problems at all frequencies [9, 10].

In this paper, a hybrid CFD-BEM technique [2, 3] is applied to predict the low Mach number flow induced noise generated by a circular cylinder immersed in a turbulent flow of Reynolds number  $Re_D = 46,000$  and Mach number  $M = 0.21$ . A large eddy simulation (LES) of the turbulent flow past the cylinder is performed to determine the fluctuating velocity field and extract

the flow noise sources. Near-field formulations for the acoustic pressure and pressure gradient based on Lighthill's acoustic analogy are then applied to calculate the propagation of acoustic waves from the flow noise sources to the body surface. The incident acoustic field is then applied to a BEM solver based on the Burton and Miller formulation to predict the radiated sound pressure scattered by the body.

### Numerical Techniques

A hybrid CFD-BEM technique is proposed to predict the flow induced noise generated by turbulent flow past a circular cylinder. The following steps are involved:

1. A large eddy simulation CFD analysis to predict the unsteady turbulent flow field around the cylinder and to extract the flow noise sources based on Lighthill's acoustic analogy;
2. The propagation of the acoustic waves generated by the flow noise sources and prediction of the near-field pressure and pressure gradient incident on the cylinder surface; and
3. Application of the incident field to a BEM model of the cylinder based on the Burton-Miller formulation and calculation of the resulting scattered acoustic field.

### Hydrodynamic Field

Turbulent flow over a circular cylinder of diameter  $D$  is simulated at a Reynolds number based on the cylinder diameter of  $Re_D = 46,000$  and a Mach number of  $M = 0.21$ . A three-dimensional circular domain around the cylinder has been modelled and analysed using OpenFOAM [18]. The turbulent flow field is simulated by incompressible LES, which solves the filtered incompressible Navier-Stokes equations given by:

$$\begin{aligned} \rho_0 \frac{\partial \tilde{u}_i}{\partial t} + \rho_0 \frac{\partial}{\partial y_i} (\tilde{u}_i \tilde{u}_j) &= -\frac{\partial \tilde{p}}{\partial y_j} + 2(\mu_0 + \mu_{SGS}) \frac{\partial}{\partial y_j} \tilde{S}_{ij} \\ \frac{\partial \tilde{u}_j}{\partial y_j} &= 0 \end{aligned} \quad (1)$$

where  $\tilde{u}_i$  and  $\tilde{u}_j$  are respectively the  $i^{\text{th}}$  and  $j^{\text{th}}$  components of the filtered velocity vector,  $\tilde{p}$  is the filtered pressure and  $\tilde{S}_{ij}$  is the rate of strain tensor of the resolved scales.  $\rho_0$  and  $\mu_0$  are the density and viscosity of the fluid medium at rest. The eddy viscosity  $\mu_{SGS}$  represents the influence of the unresolved scales on the filtered motion of the fluid. The Smagorinsky model [15] of sub-grid stresses is used here to define the eddy viscosity as

$$\mu_{SGS} = \rho_0 (C_s \Delta_g)^2 |\tilde{S}| \quad (2)$$

where  $|\tilde{S}| = \sqrt{2\tilde{S}_{ij}\tilde{S}_{ij}}$  and  $C_s$  is the Smagorinsky constant which is set to 0.1 in this work.  $\Delta_g$  is the width of the filter and here is taken to be equal to the cube root of the volume of each CFD cell. van Driest damping [17] is applied to the Smagorinsky constant  $C_s$  for CFD cells close to the wall, forcing  $\mu_{SGS} = 0$  at the wall.

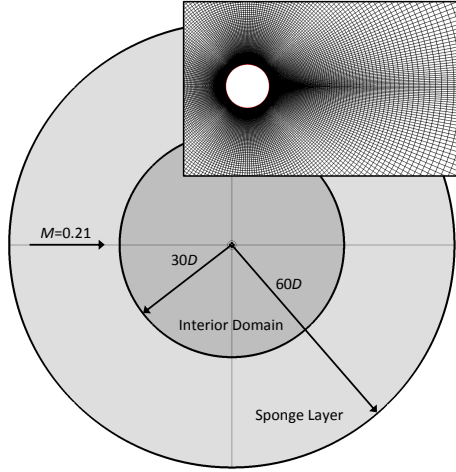


Figure 1: Domain shape and size for CFD analysis

The LES equations were solved using an iterative, segregated solution method with the pressure-velocity coupling handled using the PISO algorithm.

The model used for the LES simulation is shown in Figure 1, with the mesh topology around the cylinder inset. The interior of the computational domain extends radially for  $30D$ . A sponge layer extends radially for an additional  $30D$ . The interior domain contains 2.28 million hexahedral cells, with a cell spacing adjacent to the cylinder of  $1.3 \times 10^{-3}D$ . The sponge layer contains an additional 180,000 hexahedral cells. The cells in the sponge layer grow rapidly in the radial direction to damp out fluctuations in the velocity field and suppress generation of acoustic waves caused by vorticity leaving the domain.

A blended spatial differencing scheme was used with 95% second order central differencing and 5% second order upwind differencing. The small amount of upwind differencing was added to increase the stability of the convection equation. A second order backward implicit scheme used for the temporal discretisation. The transient simulation was executed with a time step size of  $\Delta t \frac{U_\infty}{D} = 7.2E - 3$  and was allowed to progress until the flow-field achieved quasi-periodicity. Recording of the acoustic source data then commenced and 2,560 time records were stored at an interval of  $7.2 \times 10^{-2} \frac{D}{U_\infty}$  seconds. This time interval was divided into nine equal segments with a length of 512 records and a 50% overlap. A Hann window function was applied to each segment of the time histories of the Lighthill tensor before converting them to frequency spectra.

#### Near-field Formulation for Flow Induced Noise Propagation

The propagation of the acoustic waves generated by the flow noise sources to the surface of the cylinder is resolved using formulations for the near-field pressure and pressure gradient derived based on Lighthill's analogy [2, 3]. The incident pressure  $p_a^i$  and its normal derivative  $q_{a,n}^i$  on the body are given by

$$p_a^i(\mathbf{x}, \omega) = \lim_{\epsilon \rightarrow 0} \int_{(\Omega - V_\epsilon)} \hat{T}_{ij}(\mathbf{y}, \omega) G_{h_{ij}} d\mathbf{y} \quad (3)$$

$$q_{a,n}^i(\mathbf{x}, \omega) = \lim_{\epsilon \rightarrow 0} \int_{(\Omega - V_\epsilon)} \hat{T}_{ij}(\mathbf{y}, \omega) G_{h_{ij,n}} d\mathbf{y} \quad (4)$$

where  $y_i$  is the  $i^{\text{th}}$  component of the acoustic source point position vector  $\mathbf{y}$ .  $\mathbf{x}$  is the field point where the near-field pressure and

its normal derivative are recovered.  $\Omega$  is the computational domain and  $V_\epsilon$  and represents an exclusion neighbourhood taken around the field point  $\mathbf{x}$ . This exclusion neighbourhood allows the singularities occurring when  $\mathbf{x} = \mathbf{y}$  to be regularised. The harmonic free field Green's function of the wave equation is given by

$$G_h = \frac{e^{ik_a r}}{4\pi r} \quad (5)$$

where  $i$  is the imaginary unit,  $k_a$  is the acoustic wavenumber and  $r = |\mathbf{x} - \mathbf{y}|$ . The derivative of the Green's function in the  $y_i$  direction is represented by  $G_{h_i}$ , with repeated indices indicating higher order differentiation.  $T_{ij}$  is the Lighthill tensor and is here represented by

$$T_{ij} = \rho_0 u_i u_j \quad (6)$$

where  $u_i$ ,  $u_j$  are respectively the  $i^{\text{th}}$  and  $j^{\text{th}}$  components of the velocity vector. Additional details of the formulations for the near-field pressure and pressure gradient as well as their numerical treatment can be found in Refs. [2, 3].

#### Scattering of Aeroacoustic Incident Fields using BEM

The non-homogeneous Helmholtz equation is given by [10]

$$\Delta p_a(\mathbf{x}) + k_a^2 p_a(\mathbf{x}) = -Q \quad (7)$$

where  $Q$  is an acoustic source.

Applying the method of Burton and Miller to equation (7) and combining with the incident field produced by the aeroacoustic sources yields

$$\begin{aligned} c(\mathbf{y}) p_a(\mathbf{y}) + \int_{\Gamma} G_{h_n} p_a(\mathbf{x}) d\Gamma + i\beta \int_{\Gamma} G_{h_{nn}} p_a(\mathbf{x}) d\Gamma = \\ i\rho_0 c_0 k_a \left\{ \int_{\Gamma} G_h(\mathbf{x}, \mathbf{y}) v_a(\mathbf{x}) d\Gamma - i\beta [c(\mathbf{y}) v_a(\mathbf{y}) - \int_{\Gamma} G_{h_n} v_a(\mathbf{x}) d\Gamma] \right\} + p_a^i(\mathbf{y}) + i\beta q_{a,n}^i(\mathbf{x}) \end{aligned} \quad (8)$$

where  $c(\mathbf{y})$  is a free-term coefficient and equals 1 in the domain interior and 0.5 on a smooth boundary.  $n$  is a unit vector in the direction normal to the boundary.  $\beta$  is the Burton and Miller coupling parameter.  $c_0$  is the speed of sound of the fluid medium at rest and  $v_a$  is the fluid particle velocity and is related to the normal derivative of the acoustic pressure as follows

$$q_{a,n} = \frac{\partial p_a(\mathbf{x})}{\partial n(\mathbf{x})} = i\rho_0 c_0 k_a v_a(\mathbf{x}) \quad (9)$$

In this paper, solution of equation (8) is achieved using the two dimensional AEBEM2 solver of Kirkup [7], which is based on the Burton and Miller formulation. The cylinder is discretised into 100 evenly spaced one-dimensional boundary elements.

## Results

### Unsteady Turbulent Flow Field

The flow over the cylinder is in the sub-critical regime at a Reynolds number  $Re_D = 46,000$  and a Mach number  $M = 0.21$ . Figure 2 shows an iso-surface of the  $Q$ -criterion, with  $Q = 0.5D^2/U_\infty^2$ , revealing structures in the turbulent flow. As the fluid travels over the cylinder it separates and forms a shear layer. This shear layer becomes unstable and breaks up into regions of small scale turbulence which continue to develop as they travel downstream. In the near-wake region large vortical structures associated with the coherent vortex shedding are evident. Figure 3 shows the non-dimensional spanwise vorticity  $\gamma^+ = \gamma D/U_\infty$

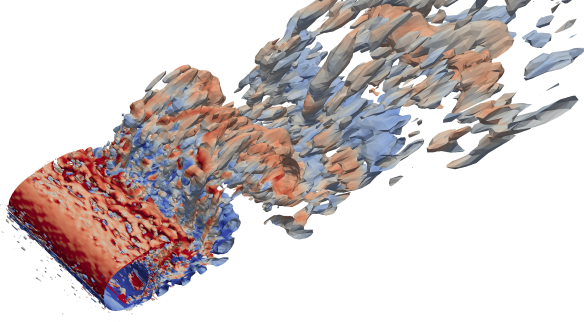


Figure 2: Flow structures over the cylinder at  $Re_D = 46,000$  and Mach number  $M = 0.21$ ; iso-surface of  $Q = 0.5D^2/U_\infty^2$

Table 1: Comparison of the Strouhal number  $S_t$ , time averaged drag coefficient  $C_{D,avg}$ , rms drag coefficient  $C_{D,rms}$  and rms lift coefficient  $C_{L,rms}$

	$S_t$	$C_{D,avg}$	$C_{D,rms}$	$C_{L,rms}$
Ref. [16]	0.19	1.35	0.16	0.45-0.5
Ref. [14]	0.187	1.24	0.1	0.54
Present work	0.216	1.06	0.065	0.43

on a plane through the centre of the cylinder's span. Spurious oscillations in the vorticity field are evident, indicating that the blending of 5% second order upwind differencing is insufficient to suppress the instabilities associated with the central differencing scheme.

Figure 4 shows the ratio of the fluctuating velocity  $u'$  to the free stream velocity  $U_\infty$  along the centreline of the cylinder wake. The results are compared with experimental measurements obtained by Szepessy and Bearman [16]. The peak of the fluctuating velocity along the centreline of the wake is an indication of the vortex formation length [16]. Figure 4 shows that the present results compare favourably with the experimental measurements, however the LES over-predicts the vortex formation length by approximately 6%. Furthermore, the magnitude of the fluctuating velocity predicted by the LES is lower than the experimental data along the most of the cylinder wake centreline. This suggests that the present LES predicts weaker turbulent fluctuations in the near-wake of the cylinder which may be caused by excessive diffusion, either from the 5% second order upwind differencing or from the eddy viscosity.

Table 1 compares the aerodynamic coefficients obtained by the present LES with the numerical results of Seo and Moon [14] and the experimental measurements of Szepessy and Bearman [16]. The Strouhal number of the present simulation is approximately 14% larger than the reference values. The mean and root-mean-square (rms) values of the drag coefficient,  $C_{D,avg}$  and  $C_{D,rms}$ , are significantly lower than the reference values. This is consistent with the weaker near-wake fluctuations observed in Figure 4. The rms value of the lift coefficient,  $C_{L,rms}$ , compares well with the experimental measurements of Szepessy and Bearman [16].

#### Scattered Sound Pressure Field

The incident field was computed using the near-field formulations for the pressure and pressure gradient given by equations (3) and (4). The scattered fields were obtained using the AEBEM2

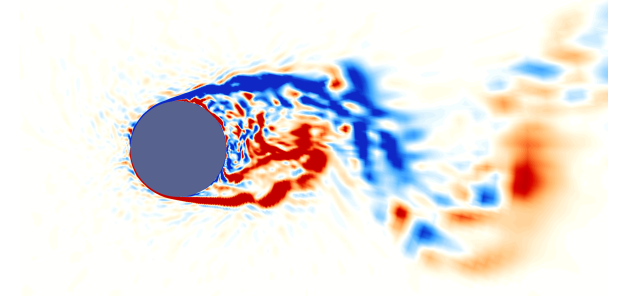


Figure 3: Non-dimensional spanwise vorticity  $\gamma^+$  on a plane through the centre of the cylinder's span. Contours are from  $\gamma^+ = -5$  (blue) to 5 (red)

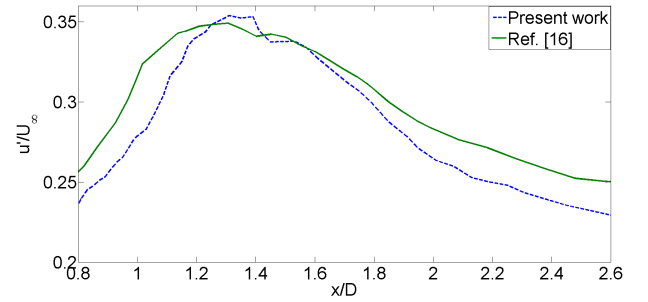


Figure 4: Ratio of fluctuating velocity  $u'$  to the free stream velocity  $U_\infty$  along the centreline of the cylinder's wake

subroutine of Kirkup [7], solving the Burton and Miller formulation. AEBEM2 is a two-dimensional solver and the far-field pressure must be converted from two dimensions to three dimensions. The following technique of Oberai et al. [11] is used to convert the pressures predicted with AEBEM2 from two dimensions to three dimensions as follows

$$p_a(x_1, x_2, x_3, \omega) \approx p_a(x_1, x_2, \omega) \frac{1+i}{2} \sqrt{\frac{k_a}{\pi r}} \quad (10)$$

where  $p_a(x_1, x_2, \omega)$  and  $p_a(x_1, x_2, x_3, \omega)$  are respectively the two and three-dimensional pressures at angular frequency  $\omega$ .

A 3D length segment of the cylinder has been simulated and the far-field pressure is modified to account for scattering by the entire span using the following correction [14]

$$SPL_t = SPL_s + SPL_c \quad (11)$$

where  $SPL_t$  and  $SPL_s$  are the sound pressure level for the entire span and simulated span, respectively, and  $SPL_c$  is a correction given by

$$SPL_c = \begin{cases} 10 \log(N), & \frac{L'_c}{L_s} \leq \frac{1}{\sqrt{\pi}} \\ 10 \log\left(\frac{L'_c}{L_s}\right) + 10 \log(\sqrt{\pi}N), & \frac{1}{\sqrt{\pi}} < \frac{L'_c}{L_s} < \frac{N}{\sqrt{\pi}} \\ 20 \log(N), & \frac{L'_c}{L_s} \geq \frac{N}{\sqrt{\pi}} \end{cases} \quad (12)$$

where  $N$  is the total number of segments and  $L_s$  is the length of the simulated span.  $L'_c$  is the spanwise coherence length and is taken from values calculated by Seo and Moon [14].

Figure 5 shows the sound pressure level for the entire span at a point directly above the mid span of the cylinder and  $r = 185D$

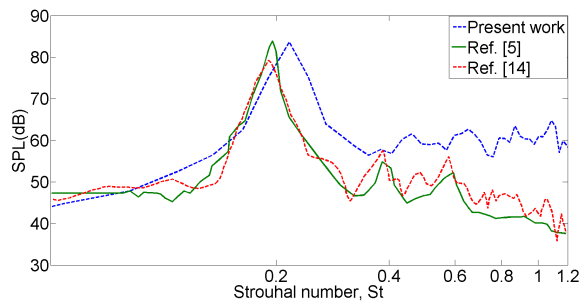


Figure 5: Sound pressure level spectrum at  $r = 185D$

from the cylinder axis. The sound pressure level is compared with numerical results presented by Seo and Moon [14] and experimental measurements obtained by Jacob et al. [5]. The peak sound pressure level associated with the vortex shedding is well captured with the hybrid CFD-BEM technique applied in this paper. Secondary peaks at higher frequencies are also predicted with the present method, however these peaks have a much higher sound pressure level than the reference results. Furthermore, the sound pressure level predicted with the present method does not decrease with increasing frequency as the reference results do. The reason for this is under investigation, however it is likely caused by the high frequency oscillations in the velocity field introduced by the central differencing scheme.

## Conclusions

A hybrid CFD-BEM technique has been proposed to predict the flow induced noise produced by low Mach number flow past a rigid body. An incompressible LES of the transient hydrodynamic flow field is performed. Acoustic sources based on Lighthill's analogy are extracted from the flow field data. The propagation of waves from the flow noise sources to the surface of the body and the resulting incident pressure and pressure gradient is calculated based on a near-field solution of Lighthill's analogy. This incident field is then combined with a BEM model of the body based on the Burton-Miller formulation to predict the scattered sound pressure field. The results from this hybrid CFD-BEM technique are presented for turbulent flow past a circular cylinder, with Reynolds number  $Re_D=46,000$  and Mach number  $M=0.21$ . The computed aerodynamic and acoustic results compare well with numerical results and experimental data from literature. The present investigation suggests that the accuracy of the results could be further improved by using less diffusive differencing schemes and by filtering the acoustic source data prior to calculating the incident field.

## References

- [1] Burton, A. J. and Miller, G. F., The application of integral equation methods to the numerical solution of some exterior boundary-value problems, *Proc Roy Soc Lon A*, **323**, 1971, 201–210.
- [2] Croaker, P., Kessissoglou, N. and Marburg, S., A unified approach to predict near and far-field acoustic pressure from Lighthill's analogy, in *18th Australasian Fluid Mechanics Conference*, Launceston, Australia, 2012.
- [3] Croaker, P., Kessissoglou, N. and Marburg, S., A CFD-BEM coupling technique for low mach number flow induced noise, in *Proceedings of Acoustics 2013*, Victor Harbor, Australia, 2013.
- [4] Curle, N., The influence of solid boundaries upon aerodynamic sound, *Proc Roy Soc Lon A*, **231**, 1955, 505–514.
- [5] Jacob, M. C., Boudet, D., Casalino, D. and Michard, M., A rod-airfoil experiment as a benchmark for broadband noise modelling, *Theor Comp Fluid Dyn*, **19**, 2005, 171–196.
- [6] Khalighi, Y., Mani, A., Ham, F. and Moin, P., Prediction of sound generated by complex flows at low Mach numbers, *AIAA J*, **48**, 2010, 306–316.
- [7] Kirkup, S. M., *The Boundary Element Method in Acoustics*, Integrated Sound Software, 1998.
- [8] Lighthill, M. J., On sound generated aerodynamically, I. General theory, *Proc Roy Soc A*, **211**, 1952, 564–587.
- [9] Marburg, S. and Amini, S., Cat's eye radiation with boundary elements: Comparative study on treatment, *J Comput Acoust*, **13**, 2005, 21–45.
- [10] Marburg, S. and Nolte, B., editors, *Computational Acoustics of Noise propagation in fluids*, Springer, Berlin, Germany, 2008.
- [11] Oberai, A., Roknaldin, F. and Hughes, T. J. R., Computation of trailing edge noise due to turbulent flow over an airfoil, *AIAA J*, **40**, 2002, 2206–2216.
- [12] Schenk, H. A., Improved integral formulation for acoustic radiation problems, *J Acoust Soc Am.*, **44**, 1968, 41–58.
- [13] Schram, C., A boundary element extension of Curle's analogy for non-compact geometries at low-Mach numbers, *J Sound Vib*, **322**, 2009, 264–281.
- [14] Seo, J. and Moon, Y., Aerodynamic noise prediction for long-span bodies, *J Sound Vib*, **306**, 2007, 564–579.
- [15] Smagorinsky, J., General circulation experiments with the primitive equations. i. the basic experiment, *Mon Weather Rev*, **91**, 1963, 99–164.
- [16] Szepessy, S. and Bearman, P. W., Aspect ratio and end plate effects on vortex shedding from a circular cylinder, *J Fluid Mech*, **234**, 1992, 191–217.
- [17] van Driest, E. R., On turbulent flow near a wall, *J Aeronaut Sci*, **23**, 1956, 1007–1011.
- [18] Weller, H. G., Tabor, G., Jasak, H. and Fureby, C., A tensorial approach to computational continuum mechanics using object-oriented techniques, *Computer in Physics*, **12**, 1998, 620–631.